Effect of Marine Stratocumulus Clouds on the Ocean-Surface Heat Budget

HOWARD P. HANSON[1,2]

Atlantic Oceanographic and Meteorological Laboratory, ERL/NOAA, Miami, FL 33149

PATRICIA L. GRUBER

Rosenstiel School of Marine and Atmospheric Science, Miami, FL 33149

(Manuscript received 27 March 1981, in final form 14 December 1981)

ABSTRACT

The mixed-layer stratocumulus model first developed by Lilly is extended to include liquid-water-dependent solar optical properties and infrared radiative fluxes. The ocean-surface heat budget under these clouds is discussed as a function of ocean temperature, wind speed and large-scale divergence.

Comparison of diurnally-varying solar forcing with daily-averaged forcing indicates the importance of the nonlinear effect of the clouds becoming thin during mid-day, when the sun is strongest. Absorption of solar energy by the cloud is responsible for this: it tends to cut off turbulent entrainment, and the cloud top becomes lower; it heats the layer, and the cloud base rises.

The ocean-surface heat budget is generally negative (oceanic heating) under these clouds, and tends to become positive as the ocean temperature is raised. The climatic implications of this negative feedback, and a similar feedback at the cloud-top level are discussed.

1. Introduction

This discussion centers on quantitative modeling of the processes through which the ocean surface heat budget is affected by the presence of stratocumulus (Sc) cloud decks. Satellite radiation budget studies (e.g., Winston *et al.*, 1979) clearly show the persistent Sc decks west of California, Peru and Angola as areas of zonally-anomalous high albedo, where the earth–atmosphere system absorbs some 20% less solar energy on an annual basis than elsewhere at the same latitudes. Theoretical radiative transfer calculations with clouds present (e.g., Schneider, 1972) show that clouds generally act as infrared (IR) insulators because of the relative coldness of their tops and their IR opacity, but the low Sc cloud tops makes them inefficient as IR "greenhouses" and the radiation budget is dominated by their relatively high albedo compared to the ocean. However, in terms of the net heat budget at the ocean surface, the radiative fluxes are only parts of the whole, since the turbulent fluxes of sensible and latent heat can be of a magnitude similar to the radiative fluxes. Therefore, atmosphere–ocean feedback studies require a consistent method of calculating both radiative and turbulent fluxes; this paper presents an extension of the mixed-layer Sc model first developed by Lilly (1968) appropriate for such calculations. The main contribution here is the inclusion in the Sc model of energetically-consistent, internally-calculated radiative fluxes (and their influence on the Sc mechanics). With some minor modifications, the radiative method used here can also be applied to trade-wind cumulus clouds; this paper concentrates on the simpler Sc case with unity-fractional cloud coverage.

The main thermodynamic variable of interest to atmosphere–ocean interaction researchers is the ocean surface temperature (OST) and much effort has been devoted to understanding feedback processes between the two media. It is intuitively clear that the OST affects the surface radiation budget, through its influence on cloud cover, as well as the turbulent heat fluxes, especially through the exponential relationship between saturation water-vapor pressure and temperature. The relative magnitudes of these influences are not obvious, however, and this paper provides an assessment of the net role of OST changes on the ocean surface heat budget for Sc conditions. It will be seen, further, that the large-scale horizontal wind divergence also plays a crucial role in the surface heat budget through its control of cloud thickness and associated cloud optical properties.

Although the calculations discussed here are confined to the stratocumulus-topped marine boundary layer, the results have a bearing on the cloud-surface temperature feedback vis-a-vis the earth–atmosphere

[1] National Research Council Resident Research Associate.

[2] Present affiliation: CIRES, Box 449, University of Colorado, Boulder, 80309

0022-4928/82/040897-12$07.00

radiation budget. Schneider's (1972) results and subsequent work by Cess (1974, 1976) showed that the IR feedback associated with clouds depends on whether it is assumed that the cloud tops occur at a specified height or that the temperature of the tops is fixed. The cloud-top height and temperature are both dependent variables in the current study, and this enables that particular controversy to be resolved for marine stratocumulus clouds.

In Section 2, Lilly's (1968) Sc model is extended to include interactive radiative fluxes. Section 3 contains results of calculations of daily averaged and diurnal solar forcing, and the heat budget. Conclusions are drawn in Section 4.

2. Model

In recent years there have been a number of papers extending and discussing Lilly's (1968) mixed-layer Sc model (Schubert, 1976; Deardorff, 1976; Kraus and Schaller, 1978a,b; Schaller and Kraus, 1978; Schubert *et al.*, 1979a,b; Kahn and Businger, 1979; Randall, 1980a,b; Deardorff, 1980; Deardorff and Businger, 1980; Lilly and Schubert, 1980; Fravalo *et al.*, 1981; Hanson, 1981, 1982; Schaller and Kraus, 1981a,b; Stage and Businger, 1981a,b; Wakefield and Schubert, 1981) but none of these has investigated the role of the model in determining the heat fluxes at the ocean surface. The Sc model derivation has been presented several times (e.g., Lilly and Schubert, 1980) and will not be repeated here. The main contribution to the topic of Sc modeling in the first two subsections below is the inclusion of cloud liquid-water dependent visible absorptance and reflectance and a sub-cloud layer infrared cooling.

In expressing the radiative fluxes, it is desirable to maintain consistency with the thermodynamic model regarding degrees of freedom (Schubert *et al.*, 1979a). The basic simplicity of the thermodynamic model (i.e., the vertically-integrated budgets of enthalpy, water and buoyancy-related turbulence) therefore constrains the radiative flux model to be highly parametric relative to state-of-the-art radiative transfer theory. The processes included here are: solar radiation absorption and reflection by the cloud and the ocean; and infrared absorption and emission by the cloud, the ocean and the water vapor in the subcloud layer. The effect of nonblack clouds, in the infrared (IR), is neglected and would be small in any case. Solar radiation absorption by water vapor in the subcloud layer is also neglected, in order to isolate the role of the cloud. Including this process would exacerbate the results discussed in Sections 3a,b.

a. Solar radiation

The solar radiation and reflection by the clouds is modeled using the fourth-order polynomials presented by Liou and Wittman (1979). They give regression constants for various cloud types from which cloud absorptance, reflectance and transmittance can be calculated as functions of cloud liquid-water content (LWC) and the solar zenith angle cosine (μ). The LWC is defined as

$$\text{LWC} = \int_{z_C}^{z_B} \rho\, l\, dz,$$

where l is the liquid water mixing ratio of cloud droplets, ρ is the air density and z is height; z_B and z_C are the cloud-top and base levels, respectively. The mixed-layer Sc model predicts the layer-averaged total water mixing ratio $r = q + l$, where q is the water-vapor mixing ratio (saturated in the cloud) and $l = 0$ below cloud base; and the layer-averaged moist static energy, $h = c_pT + Lq + gz$, where c_p, L and g are the specific heat of air at constant pressure, the latent heat of condensation and the acceleration of gravity, respectively, and T is the absolute temperature. The model also predicts z_c as a lifting condensation level (e.g., Deardorff, 1976) and z_B using a simplified turbulence closure (see Section 2c below). Using the constraint that h and r are vertically constant and a linearization of the Clausius-Clapeyron equation, the cloud-top liquid water mixing ratio l_B can be found. Since there is no subcloud transition in the Sc model, $l_C = 0$ and $r_C = q_C = q_C^*$ (superscript asterisk denoting saturation). The LWC is therefore, to a first approximation,

$$\text{LWC} = \hat{\rho} l_B (z_B - z_c)/2$$

where $\hat{\rho}$ is a vertically-averaged density. Typically, the model gives $l_B \leqslant 0.001$, so that, for a 500 m thick cloud, LWC $\leqslant$ 275 gm^{-2} producing a maximum cloud reflectance $R_c \simeq 0.65$, absorptance $A_c \simeq 0.15$ and minimum transmittance $T_c \simeq 0.20$ for a 30° solar zenith angle (Liou and Wittman, 1979).

Given the optical properties of the cloud alone, the relevant optical properties of the Sc-topped layer can be found by correcting for multiple reflections between the cloud base and the surface (e.g., Schneider and Dickinson, 1976); this correction is small, since the ocean-surface albedo is taken to be 9% (Ivanoff, 1977). Further, because the cloud cover is unity, no zenith angle dependence is introduced for this quantity (all the solar radiation in the subcloud layer is assumed to be diffuse). With the net reflectance and absorptance, R_{net} and A_{net}, an effective optical depth for the cloud can be found by inverting

$$\begin{aligned} F_{\text{sol}C} &= F_{\text{sol}B}[1 - R_{\text{net}} - A_{\text{net}}] \\ &= F_{\text{sol}B}[1 - R_{\text{net}}] \exp[-(z_B - z_C)/\tau_{\text{sol}}], \end{aligned}$$

where $F_{\text{sol}B}$ is the downward solar flux at z_B, $F_{\text{sol}C}$ is the net solar flux at z_C and τ_{sol} is the cloud optical depth (absorption and scattering, except for the ocean surface, being neglected below z_C). The stip-

ulation of an exponential net solar flux profile follows Deardorff (1976) and is consistent with the treatment of IR radiation below. For the typical numerical values above, $\tau_{sol} \geq 850$ m, restricting the ability of the solar radiation to interact directly with the cloud turbulence energy budget (in the entrainment closure), but the contribution to the total energy budget will be seen below to decrease the turbulent production, in agreement with numerical results (Oliver *et al.*, 1978).

b. *Infrared radiation*

Infrared radiation is an important forcing mechanism for Sc clouds, as pointed out by Lilly (1968), particularly at the cloud top where radiative flux changes of the order 50 W m^{-2} occur over a few tens of meters. In previous Sc modeling studies using the mixed-layer model (e.g., Schubert *et al.*, 1979a; Randall, 1980b), IR transfer below the top part of the cloud has been neglected. It is included here to account for the possibility of subcloud layer heating or cooling (e.g., Fravalo *et al.*, 1981; Stage and Businger, 1981a).

In this paper, the ocean surface, the cloud base and the cloud top are assumed to radiate as blackbodies at their respective temperatures, and the subcloud layer is assumed to act as a grey body, with emissivity (for water vapor only) from Sasamori's (1968) parameterization. The net IR flux at the ocean surface thus depends on the OST and the downward flux from the cloud base and the subcloud layer. Similarly, the net IR flux at cloud base depends on the cloud-base temperature and the upward flux from the surface and the subcloud layer. The subcloud layer IR cooling rate is then the net flux difference across the layer divided by the layer depth. The net IR flux at the cloud top is found as in Schubert *et al.* (1979a).

Much discussion among the papers cited at the beginning of this section concerns the precise structure of the cloud-top IR radiation divergence. Lilly (1968) originally proposed that it occurs just above the limit of saturated air (i.e., in the inversion) so that, in the limit of a zero-order (discontinuity) inversion,

$$\overline{w'h'_B} = -w_e \Delta h - \frac{1}{\rho_B} \Delta F_{IR}^{CT},$$

where $\overline{w'h'_B}$ is the turbulent flux of moist static energy at the cloud top (within the saturated air), $\Delta h = h_u - h_B$ with h_u the (dry) upper air value, w_e the entrainment rate and ΔF_{IR}^{CT} the IR flux "jump" from a value [0(50 W m^{-2})] above the cloud to zero within the cloud. Since Lilly (1968) did not develop an explicit entrainment closure, but rather defined maximum and minimum limits on the entrainment, it was not until Deardorff's (1976) entrainment rate closure that the importance of precisely where ΔF_{IR}^{CT} occurs became an issue. Deardorff suggested that, in fact, ΔF_{IR}^{CT} must occur across a finite depth, because of the nonhorizontally uniform nature of the upper limit of the saturated air (i.e., the cloud top is not actually perfectly flat). The distribution of ΔF_{IR}^{CT} has also been discussed by Schubert *et al.* (1979a), Kahn and Businger (1979), Deardorff and Businger (1980) and Stage and Businger (1981a). In the approach used here, all the cloud-top IR flux divergence is assumed to occur below the mean inversion, distributed over a depth of a few tens of meters (Randall 1980b; Deardorff and Businger, 1980). As noted by Stage and Businger (1981b), this causes the model to predict relatively shallow layers because IR flux divergence within the mean inversion is more efficient at promoting entrainment. The cloud thickness, however, is not strongly affected by this assumption and the heat budgets shown below are rather insensitive to cloud-top IR flux details.

In this paper, the exponential IR flux profile suggested by Kahn and Businger (1979) is adopted, using an *e*-folding length of 20 m. (Increasing and decreasing this length by factors of two causes minor decreases and increases, respectively, in the entrainment rate, but the model is relatively insensitive to this parameter). The model used here, therefore, has exponential radiative flux profiles; these are shown with the corresponding buoyancy flux in Fig. 1a (taken from the average of the NH case discussed fully below). The same *e*-folding length for the IR flux is also used at the cloud-base level. In principle, this could be calculated, but, as that would involve details about the cloud droplet spectrum far beyond the basic simplicity of the mixed-layer Sc model, it is specified here.

c. *Boundary conditions and closure*

As with all mixed-layer Sc models, it is necessary to specify conditions above the cloud top: specifically, the upper-level moist static energy, water vapor and downward IR flux profiles. In the calculations presented below, the Northern Hemisphere cases use the upper quantities from Schubert *et al.* (1979a) and the Southern Hemisphere cases use profiles from Steiner and Schubert (1976). For the Northern Hemisphere:

$$h_u = 314.4 + 1.87 \cdot 10^{-3} z_B \text{ kJ kg}^{-1},$$

$$q_u = 4.38 - 6.14 \cdot 10^{-4} z_B \text{ g kg}^{-1},$$

$$F_{IR1u} = 339.4 - 3.98 \cdot 10^{-2} z_B \text{ W m}^{-2},$$

and Southern Hemisphere:

$$h_u = 305.24 + 5.21 \cdot 10^{-3} z_B \text{ kJ kg}^{-1},$$

$$q_u = 3.22 - 2.53 \cdot 10^{-4} z_B \text{ g kg}^{-1},$$

$$F_{IR1u} = 324.1 - 3.56 \cdot 10^{-2} z_B \text{ W m}^{-2},$$

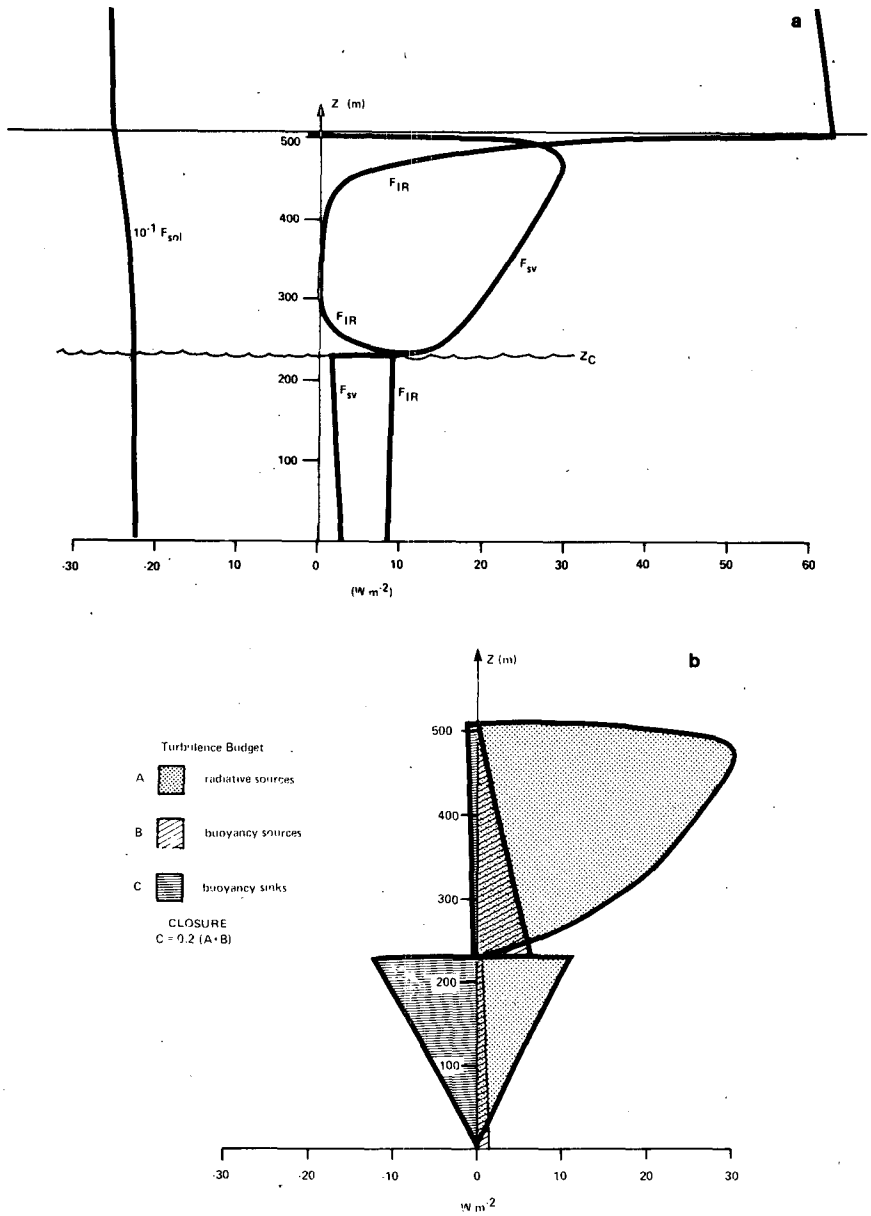

FIG. 1. (a) Vertical profiles of radiative and buoyancy fluxes, from daily average of NH case. (b) Balance of turbulent production and destruction used in entrainment closure.

with z_B in m. The Southern Hemisphere profiles are cooler, drier and more stable than the Northern Hemisphere profiles, reflecting the winter-summer differences for July.

In addition, the solar radiation calculation requires an effective solar constant. For this purpose, the direct beam solar flux is specified (diffuse solar radiation from above is neglected) as a function of latitude and month (July), with a crude correction for upper atmospheric Rayleigh backscattering, and ozone and water vapor absorption using the parameterizations developed by Lacis and Hansen (1974). Calculations below compare the differences between averages of diurnal solar forcing with daily-averaged solar forcing; nonlinearities inherent in the zenith angle dependence of the cloud optics will be seen to present basic research challenges for long-time-step climate investigations.

Also specified in this paper, as lower boundary conditions, are the OST and the surface wind speed. As is common in models of this type, the surface turbulent fluxes are obtained using the bulk aerodynamic formulas, with a transfer coefficient for both heat and water vapor of 1.4×10^{-3}. In so far as both the wind speed and the transfer coefficient are specified, the exact value of the latter is unimportant,

although it may in fact be lower for the relatively stable conditions under Sc decks. Schubert (1976) dealt with this issue by specifying the product of the two: in the present analysis, the effect of lower transfer coefficients may be inferred by simply adjusting (upward) the wind speed.

As with the cloud-top IR flux, the entrainment closure for mixed-layer Sc models has been a matter of some discussion. For the main results below, a closure based on the oceanic mixed-layer entrainment closure of Niiler and Kraus (1977), and recently proposed for use in the atmospheric boundary layer by Stage and Businger (1981a,b) has been used. This relates potential energy production by negative buoyancy fluxes throughout the layer to a fraction of the turbulent kinetic energy produced by positive buoyancy fluxes throughout the layer (Hanson, 1982). It differs from the closure suggested by Stull (1976), Kraus and Schaller (1978a) and Randall (1980b), in that the level(s) of zero-buoyancy flux need not be found. (With the radiative flux formulation used here, this could conceivably be three levels.) Fig. 1b shows the sources and sinks of turbulence associated with the flux profiles in Fig. 1a. Note that the "negative area" under the virtual static energy flux curve in Fig. 1a is quite small (just below the cloud top), while the areas in Fig. 1b show substantial turbulent destruction by negative buoyancy forces below cloud base, as well as production in the upper part of the subcloud layer by the IR cooling.

In all the results below, the Sc model has been solved numerically as a time-dependent initial value problem using a fourth-order Runge-Kutta procedure and 72-bit arithmetic. The cloud-base level and radiative fluxes (which are strongly model-dependent) are solved iteratively four times during each 20 min time step until the model has reached a cyclic steady state.

3. Results

a. Diurnally-forced behavior

Before a discussion of the heat budgets, it is useful to examine the model behavior for diurnal forcing. Two cases are presented, each using a solar declination of 20°N, wind speed 7 m s^{-1}, large-scale divergence of 3.5×10^{-6} s^{-1} and upper-air ozone and water vapor pathlengths of 0.25 and 0.5 cm, respectively. The Northern Hemisphere (NH) case takes the OST = 17°C at latitude 30°N and the Southern Hemisphere (SH) case takes the OST = 15°C at latitude 20°S. The daily-averaged effective solar constants are 451.7 W m^{-2} and 287.1 W m^{-2}, the SH case being the smaller.

Fig. 2 shows (top to bottom) the cloud top and base variation, the layer-averaged moist static energy (h) and total water (r) and the net radiative forcing and incident solar flux as functions of local time for

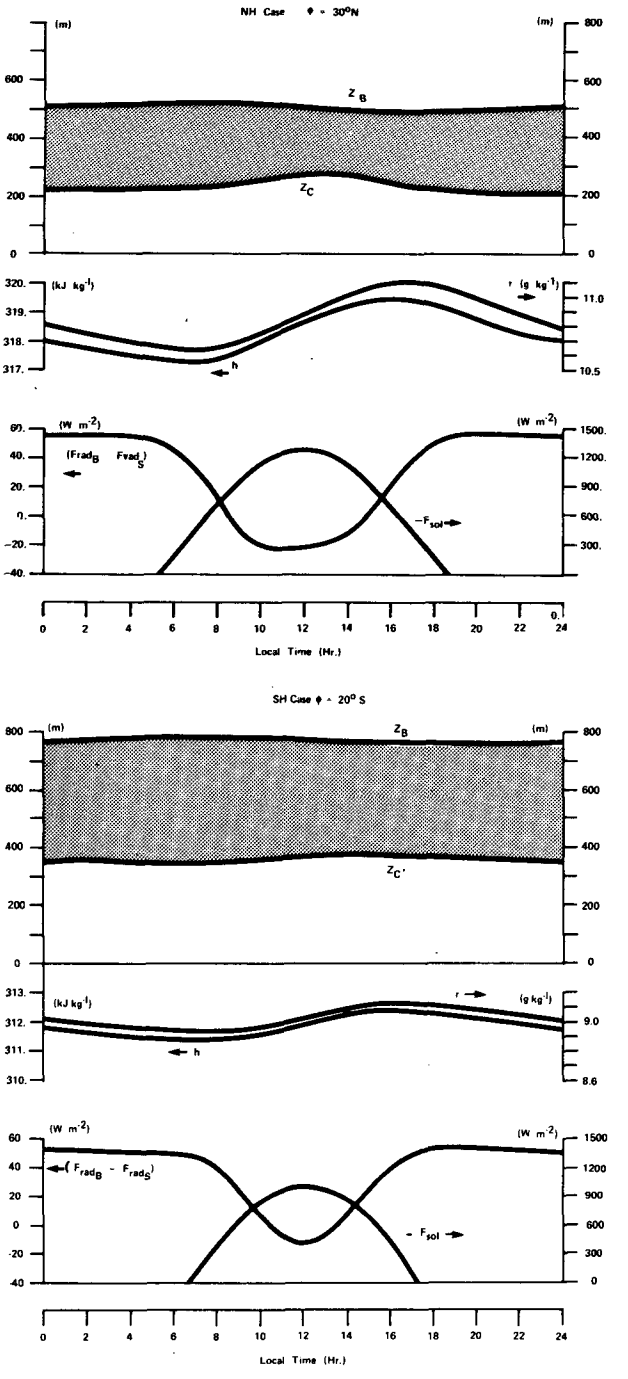

FIG. 2. (a) NH and (b) SH cases showing diurnal variations of cloud geometry, moist static energy and total water, and radiative forcing and solar flux.

the NH (a) and SH (b) cases. Even though the SH case is for a lower OST, the layer is deeper and the cloud is thicker because there is less solar energy absorbed by the cloud. During mid-day, the solar energy absorption decreases the energy available for entrainment, and the cloud top lowers. The absorption within the cloud also warms the layer, and the

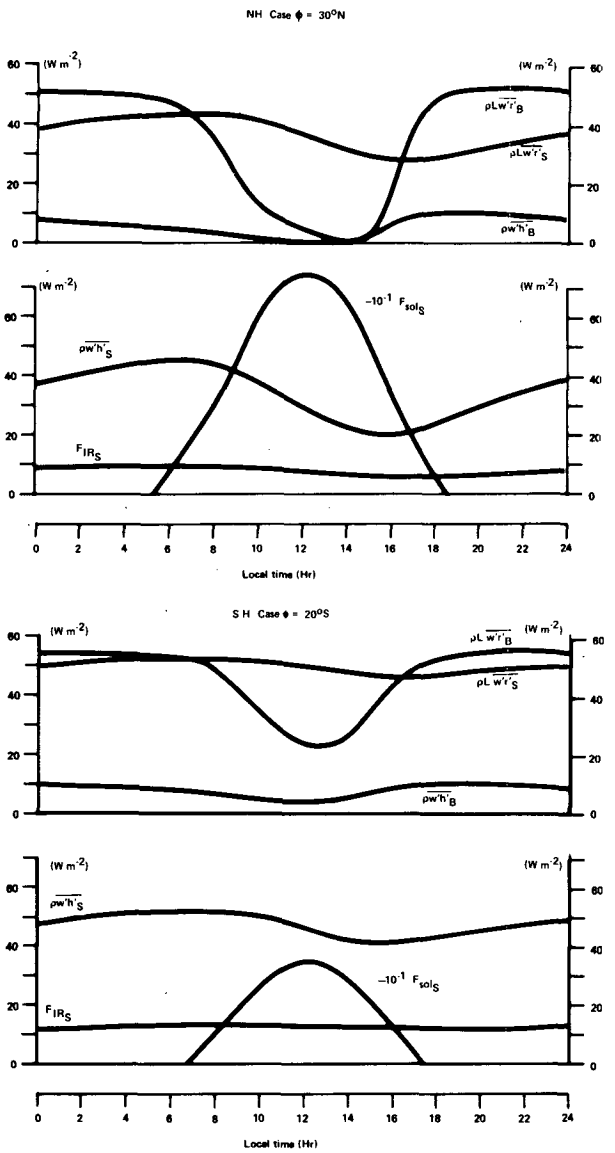

FIG. 3. (a) NH and (b) SH case results showing diurnal variation of cloud-top fluxes of moist static energy and water and surface latent heat flux; and components of the surface heat budget.

cloud base lifts; this produces a thinner cloud during mid-day, when the sun is strongest, in agreement with Oliver *et al.*'s (1978) numerical results (their Fig. 9) and in contrast to the diurnal cases discussed by Schubert (1976), who specified the solar absorption at the cloud top.

The moist static energy and total water variations are consistent with the variation of the cloud geometry. During mid-day, when the cloud becomes thinner, the moist static energy increases faster than the water and the layer warms (the left and right scales for h and r in Fig. 2 are energetically consistent). The moist static energy content lags the solar flux by ~4 h, and the moisture content lags the moist static energy by <1 h. The net radiative forcing (F_{rad_B}–F_{rad_S}) includes both infrared and solar radiations, and the NH case shows clearly the nonlinear effect of the solar maximum occurring at the time when the cloud is thinnest. This effect is present in the SH case at a much reduced level.

Fig. 3 shows (top to bottom) the cloud-top fluxes of moist static energy, moisture (in energy units) and the surface moist static energy, infrared and solar fluxes as functions of local time for the two cases. The surface turbulent fluxes reflect the diurnal variations of moist static energy and water content in the layer. The NH cloud-top fluxes become zero for ~45 min just after noon because the absorption of solar energy is strong enough to cut off the entrainment at the cloud top altogether. Although the SH cloud-top fluxes are smallest during mid-day, the solar energy absorption is not strong enough to stop turbulent entrainment.

At the surface, the net IR flux for the two cases is rather small and has little daily variation. The insulating effect of the clouds is evident in these low IR flux values: the upward blackbody radiation from the ocean minus the downward flux at the ground (i.e., σT_s^4 − 339.4 for the NH case) is about six times larger than the IR fluxes in Fig. 3. Another important point concerns the commonly-used Brunt formula for the surface IR flux (e.g., Hastenrath and Lamb, 1978). The averaged surface IR fluxes for the NH (SH) cases in Fig. 3 are 8.6 (12.7) W m^{-2} compared to 21.5 (41.9) W m^{-2} which would be obtained by use of the Brunt formula.

b. *Comparison with daily-averaged forcing*

For climate investigations it is, of course, useful not to have to calculate the diurnal cycle. In order to compare the effects of averaging the diurnal cycles discussed above with steadily forced cases, the model was run to equilibrium using identical solar flux at the top of the layer (these results, in fact, provided initial conditions for the diurnal cases above).

It is not sufficient to stipulate the solar flux for these calculations, as the radiative properties of the cloud are strongly zenith-angle dependent (Liou and Wittman, 1979). Moreover, the simplified upper-air optics used here, from Lacis and Hansen (1974), are also zenith-angle dependent. Sellers (1965, p. 16) gives a formula by which a *daily-averaged zenith angle cosine* can be found, but this is biased due to night time when solar radiative transfer is irrelevant. By comparison of: a) calculations using a *daytime-averaged zenith angle cosine,* $\tilde{\mu}$, (which is the daily-averaged from Sellers divided by the fractional day length) in the absorption and scattering parameterization of the upper air optics, with b) averages of diurnally forced calculations, with $\mu(t)$, it has been found that the solar flux incident at the cloud top can be made to agree to within better than 0.5%. For

TABLE 1. Comparison of averages of diurnal forcing with daily averaged forcing.

Case/ Forcing	Z_B (m)	Z_C (m)	$\overline{\rho w' h_S'}$ (W m^{-2})	F_{IR_S} (W m^{-2})	F_{sol_S} (W m^{-2})	F_{net_S} (W m^{-2})	$A_{S_{net}}$	R_{net}
NH/Daily	509.1	232.7	34.7	8.2	−228.3	−185.4	0.505	0.435
NH/Avg.	531.2	243.0	35.6	8.4	−188.5	−144.5	0.356	0.522
SH/Daily	774.1	359.2	46.6	12.0	−90.5	−31.9	0.315	0.629
SH/Avg.	805.9	363.7	48.8	12.5	−74.6	−13.3	0.163	0.696

the daily-average forcing cases, then, $\tilde{\mu}$ has been used in Liou and Wittman's (1979) cloud optics. This notwithstanding, the nonlinear effect of the maximum solar flux coinciding with the thinnest cloud causes large differences in the results.

Table 1 shows the results of averages of daily forcing and daily averaged forcing. Negative fluxes indicate ocean-surface heating; $A_{S_{net}}$ and R_{net} are the ocean-surface absorption and layer reflectance including multiple reflections, as discussed in Section 2a. The cloud-top heights differ by <5%, and the turbulent and IR fluxes are in reasonably close agreement, but the solar flux at the surface is ~17% less for each of the daily-averaged forcing cases. The net surface flux (F_{net_S}) is thus substantially biased by the nonlinearities of the cloud optics. The optical properties in the last two columns of Table 1 show that the net surface absorptance is strongly under-predicted by use of daily-averaged forcing and that the reflectance is over-predicted. No attempt is made here to introduce further parameterizations into the daily-averaged forcing model to resolve these differences. The results below are taken from averages of the daily forcing cases.

c. *Ocean-surface heat budget*

Figs. 4 and 5 show daily averages of the ocean-surface fluxes of infrared, sensible and latent heat (Figs. 4a, 5a), the solar flux into the ocean (Figs. 4b, 5b) and the net ocean surface heat budget (Figs. 4c, 5c) as functions of OST for two values of wind speed and divergence. The IR and turbulent fluxes increase with increasing OST; most of this is due to the increased latent heat flux. These upward surface fluxes are somewhat increased with increasing wind speed and large-scale divergence. The solar flux (downward) into the ocean (Figs. 4b, 5b) decreases as the OST is increased; this is due to the increase in cloud LWC and the net layer reflectivity as more water is evaporated into the boundary layer. The solar flux decrease is largest for combinations of wind speed and divergence which produce the deepest layer. Note that, in each hemisphere, the $V_{10} = 3.5$ m s^{-1}; $\bar{D} = 5.0\ 10^{-6}$ s^{-1} (case a) has very little surface-temperature dependence. Here, the wind speed is so low that the surface evaporation is suppressed relative to the subsidence of dry air from above. Even though the cloud-top height z_B increases with the OST, the cloud-base z_C also rises, maintaining a cloud of nearly constant thickness. Lower wind speeds and higher divergences than this are of questionable realism for large horizontal scales, but it is conceivable that a combination of circumstances could produce a cloud which would allow more solar flux into the ocean for higher OST's. However, no case has been found in which this increased oceanic heating would be larger than the increased oceanic cooling shown in Figs. 4a and 5a (as long as the Sc deck does not break up).

The net surface fluxes (Figs. 4c, 5c) behave similarly, with the Northern Hemisphere (Fig. 4c) exhibiting a stronger OST dependence due to the greater amount of solar energy incident on the layer. The main point to be noted here is the fact that, for all cases

$$\frac{\partial F_{net_S}}{\partial T_S} > 0$$

(with $F_{net_S} < 0$ giving oceanic heating). This implies a *negative feedback*, because, in the absence of changes in oceanic processes, small perturbations in the OST will tend to be damped out. The strength of the feedback depends on large-scale conditions external to the model, and as suggested above, for very suppressed, calm situations, the feedback could be very weak. Moreover, the strength also depends on the conditions above the boundary layer through their effect on the cloud-top height and thickness. Therefore, while no definitive statement about the strength of the feedback can be made here, it is shown to be negative.

The main interhemispheric difference evident between Fig. 4c and Fig. 5c is, of course, the greater net heating for the Northern Hemisphere, because it is summer there. It is also of interest to note that even in the Southern Hemisphere winter, there is a tendency for oceanic heating under the Sc deck. The relatively low OST's are associated with low surface turbulent fluxes, and the cloud suppresses the surface IR flux. Even though the cloud reflects a substantial fraction of the incoming solar flux, enough penetrates to the ocean to dominate the upward heat transfer at the surface, except for cases of very deep clouds and high OST's. That the ocean is being heated at the surface in winter simply implies a process in the

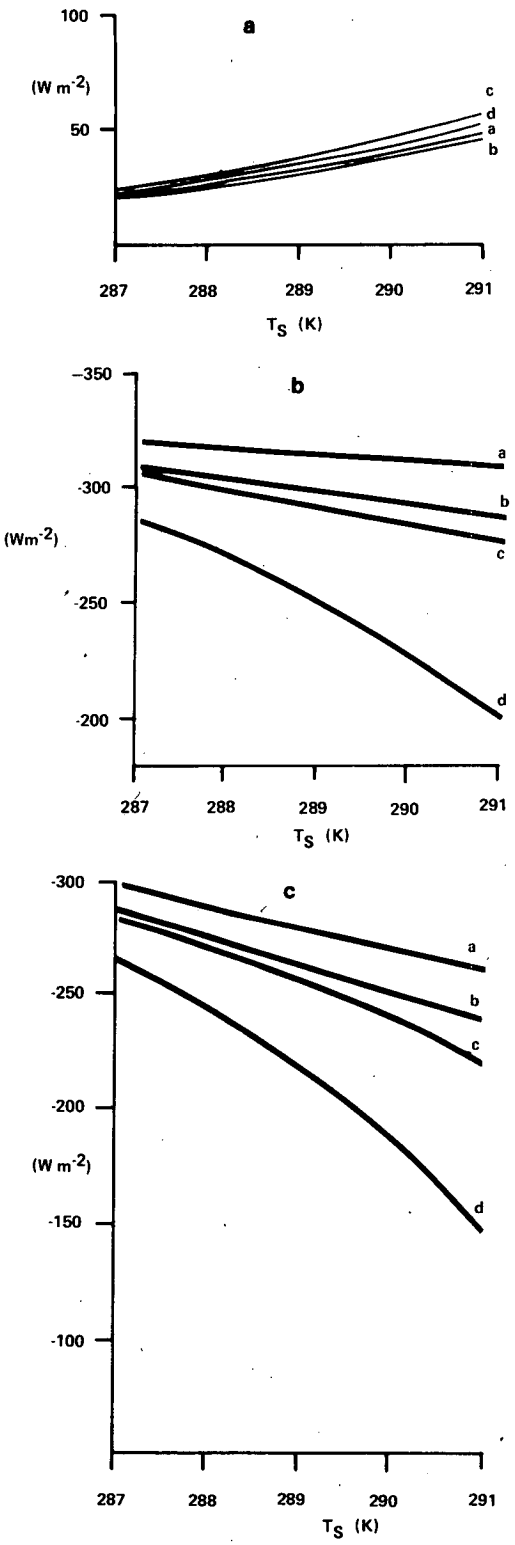

FIG. 4. Surface fluxes at 30°N for July declination *vs.* OST for two values of wind speed and divergence. (a) Sensible plus latent plus infrared flux out of the ocean. (b) Solar flux into the ocean. (c) Net surface flux. Curve (a) takes $v_{10} = 3.5$ m s^{-1}, $\bar{D} = 5.0 \times 10^{-6}$ s^{-1}; (b) takes $v_{10} = 3.5$ m s^{-1}, $\bar{D} = 3.5 \times 10^{-6}$ s^{-1}; (c) takes $v_{10} = 7$ m s^{-1}, $\bar{D} = 5 \times 10^{-6}$ s^{-1}; (d) (the "standard") takes $v_{10} = 7$ m s^{-1}, $\bar{D} = 3.5 \times 10^{-6}$ s^{-1}.

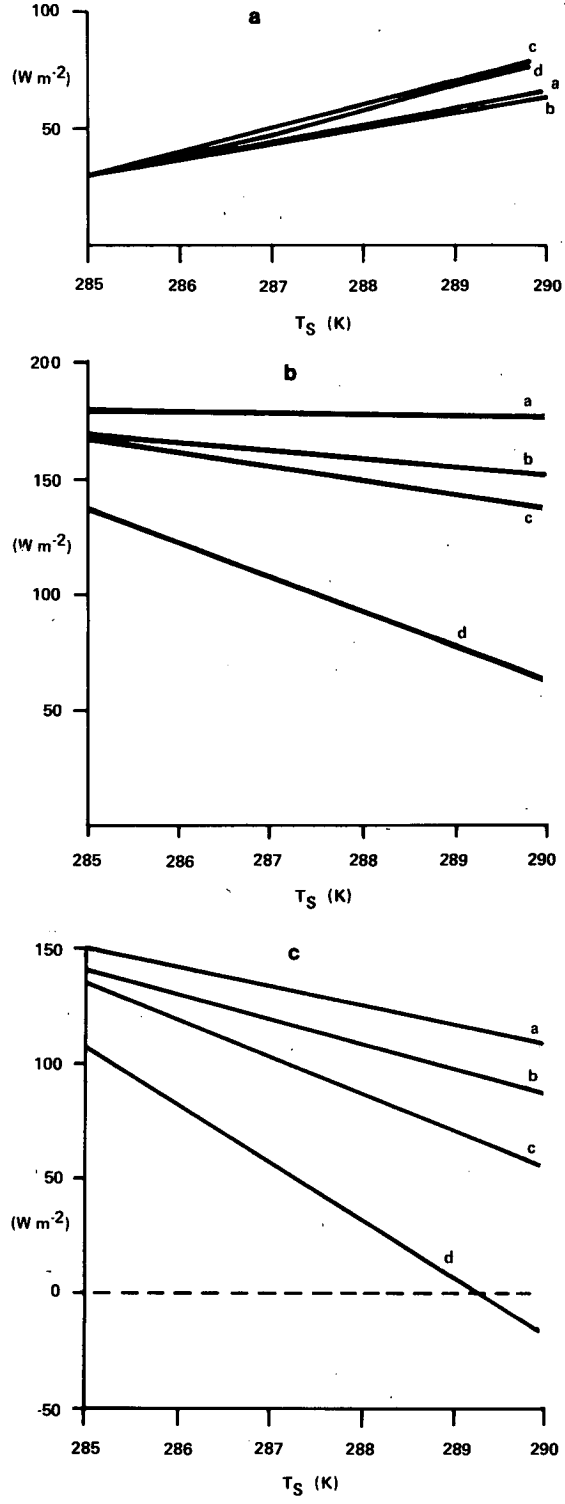

FIG. 5. As in Fig. 4 except for the Southern Hemisphere at 20°S.

ocean which maintains the OST cooler than it would otherwise be: west of South America, this would be the cold, upwelling current system which supplies the nutrient-rich fisheries off Peru.

d. Climatic implications

Climate modelers have for some time been concerned with feedback processes involving clouds, radiative transfer and the surface temperature [see Schneider and Dickinson (1974) and Ramanathan and Coakley (1978) for reviews]. Clouds interact with the radiation budget through modification of the planetary albedo and the outgoing IR flux. In low latitudes, the increased albedo of clouds tends to cool the earth–atmosphere system while the IR flux-effect tends to warm the system (Schneider, 1972). The net effect is not well-understood, however, because the relationship between cloud cover and surface temperature is unknown. In global-average studies, this problem is particularly acute since regional differences in the processes affecting cloud cover are not resolved. Even general circulation models resolve horizontal and vertical scales much larger than the scales of individual clouds, and cloud parameterizations are based on grid-scale relative humidity and vertical motion (Schneider *et al.*, 1978; Wetherald and Manabe, 1980). These parameterizations, however, restrict the radiative properties of the clouds by assignment of fixed optical properties and cloud-top heights (or temperatures). Even the sign of the net feedback is unclear (Cess, 1976).

As an alternative to parametric approaches, it seems useful to investigate climatic implications of various types of clouds individually. In doing this, the surface temperature–radiation budget feedback cannot be directly assessed since realistic equilibrium surface temperatures cannot be obtained and changes in the upper atmosphere are unknown. In the previous section it was seen that the ocean-surface heat budget under Sc decks tends to be positive (ocean heating), with negative feedback with respect to OST, due to thicker clouds and increased evaporation for higher OST's. To the extent that processes above the cloud top can be considered unchanged, and oceanic advection can be ignored, these results apply to the earth–atmosphere column.

In general circulation models, the albedo-feedback depends entirely on areal cloud coverage. The Sc deck studies here assume unity fractional coverage; the albedo-feedback is due to variable cloud optical properties controlled by the cloud LWC (Paltridge, 1980). The IR flux feedback in parametric models depends on the cloud-top assumptions (whether the top altitude or temperature is fixed); both of these quantities are dependent variables in the present model. Unlike the surface heat budgets discussed previously, here only upward radiative fluxes are considered. Figs. 6 and 7 show changes in the heat budgets from the two standard cases discussed in Sections 3a,b. Lower values of the upward flux at the cloud top imply heating of the Sc layer and the ocean, relative to the two standard cases.

Fig. 6 shows variations in the solar flux reflected

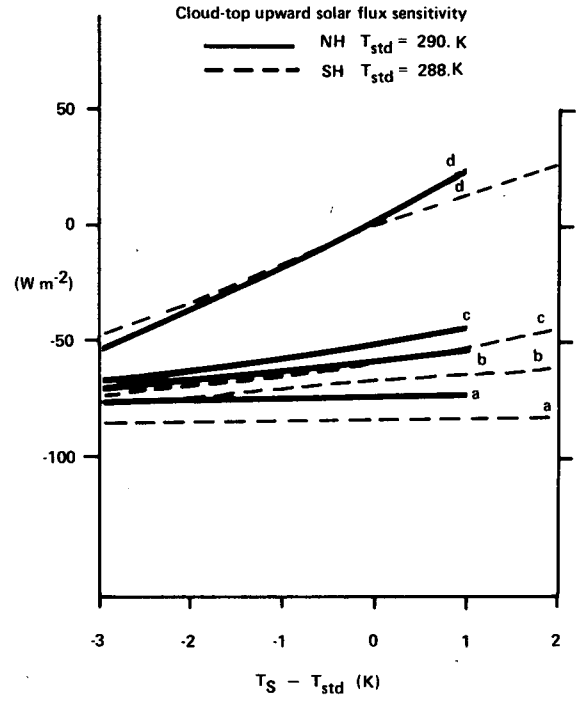

FIG. 6. Differences in reflected solar radiation as a function of OST from the two standard cases for conditions in Fig. 4.

by the Sc layer. In all cases, surface temperature increases are associated with increased solar flux reflection. As before with the surface flux, this implies a negative feedback, the strength of which depends on the conditions specified. The feedback is weaker for low wind speeds since the layer is less strongly coupled to the OST (in the bulk formulae). Fig. 7 shows the sensitivity of the upward IR flux from the clouds (this is the blackbody flux at the cloud-top temperature). Note that the ordinate in Fig. 7 is stretched by a factor of ten relative to Fig. 6; this is in order to show clearly the negative feedback of the IR flux with respect to the OST. In particular, it is useful to inquire about the relevance of common assumptions used in radiativé–convective and general circulation models. Let the cloud-top temperature be represented by

$$T_B = T_S + \Gamma z_B$$

and the upward IR flux at the cloud top

$$F_{\mathrm{IR}B\uparrow} = \sigma T_B^4 .$$

Hence,

$$\frac{\partial F_{\mathrm{IR}B\uparrow}}{\partial T_S} = 4\sigma(T_S + \Gamma z_B)^3\left(1 + \Gamma \frac{\partial z_B}{\partial T_s}\right);$$

for simplicity, the lapse rate Γ is assumed to be fixed, and the surface temperature T_s is taken to be the OST. (This is reasonably valid for Sc situations with small surface sensible heat flux, but is invalid for air mass modification cases.) The use here of the partial derivative is crucial, implying that everything except

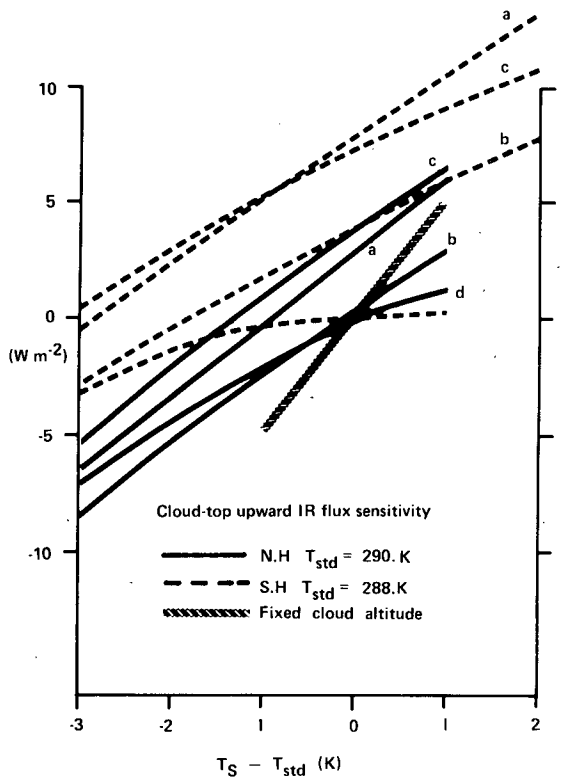

FIG. 7. Differences in upward cloud-top IR flux as function of OST from the two standard cases. Dotted line is the behavior of the FCA parameterization.

the OST is held constant; consequently, it cannot be expected that values deduced here will agree with those from radiative–convective model studies.

The assumption made in parametric cloud models of fixed cloud temperatures (FCT) takes T_B = constant and clearly $\partial F_{IRB\uparrow}/\partial T_S = 0$. The assumption of fixed cloud altitude (FCA) takes $\partial z_B/\partial T_s = 0$. Fig. 7 shows that the FCT assumption is incorrect for most of the Sc clouds calculated here. In fact, it is easily inferred, for the FCT, that $(\partial z_B/\partial T_S)$FCT $= -\Gamma^{-1} \approx 150$ m K^{-1} (using $\Gamma = -6.5$ K km^{-1}); this is consistent with calculations made for Figs. 4–7, where $\partial z_B/\partial T_S$ from the Sc model is much lower than the FCT assumption, although still positive, and $\partial F_{IRB\uparrow}/\partial T_S$ is positive. Physically, the negative feedback occurs because, as the OST increases, the layer warms up and more energy is available for entrainment and a deeper layer. However, in the turbulent energetics, 80% of that extra energy is dissipated and the extra entrainment is not strong enough to lower T_B (by increasing the layer depth) faster than the overall warming.

In the FCA assumption, $\partial z_B/\partial T_S = 0$ and $\partial F_{IRB\uparrow}/\partial T_S = 4\sigma(T_S + \Gamma z_B)^3$. The dotted line on Fig. 7 shows this sensitivity for the SH(d) curve at T_S = 288 K, the least negative feedback. The FCA assumption thus exhibits stronger negative feedback than the Sc model; this is also true for the other cases shown in Fig. 7. Therefore the Sc model shows an upward cloud-top IR flux dependence which is between that of the FCA and FCT assumptions.

4. Conclusion

a. Summary

Lilly's (1968) cloud-topped mixed-layer model, using the turbulence closure introduced by Stage and Businger (1981a,b), has been extended to include interactive radiative fluxes. Solar fluxes are calculated using Liou and Wittman's (1979) parameterizations of cloud optical properties with the further assumption of an exponential in-cloud solar flux profile. IR fluxes are calculated by assuming that the ocean surface and the cloud top and base emit as blackbodies, and that the subcloud layer emits as a grey body, using Sasamori's (1968) parameterization for water-vapor emissivity. The cloud-top and base IR flux is further taken to be distributed exponentially within the cloud using an e-folding length of 20 m. With these extensions, the Sc model has been used to examine the sensitivity of the ocean surface heat budget to changes in external parameters, notably the OST.

The diurnal behavior of the layer reveals an important nonlinearity. The cloud transmits the most solar radiation (when it is thinnest) during midday, coinciding with the maximum of available solar radiation. Comparison of the diurnally-forced layer with the daily-averaged forcing case reveals that the latter underpredicts ocean-surface heating by ~20%. Sub-cloud absorption of solar radiation was neglected here; its inclusion would further strengthen this nonlinearity. Long time-step climatic investigations thus require further parameterization efforts.

The behavior of the ocean surface and cloud-top heat budgets (the latter concerning only upward radiative fluxes) is such that a negative feedback between the cloud and the OST is implied. The strength of the feedback depends on large-scale conditions, and is generally stronger when the layer is strongly coupled to the ocean surface, e.g., by high wind speeds and low large-scale divergence. The surface heat budget is generally negative (oceanic heating), consistent with the maintenance of low ocean temperatures under the coastal Sc decks by cool ocean currents.

The strength of the cloud-top heat budget feedback is between the feedback implied by the two common parameterizations (fixed cloud temperature and fixed cloud altitude) used in numerical models. Fixing the cloud temperatures actually implies no cloud-top IR feedback, and fixing their altitudes gives too strong a negative feedback. This is consistent with the strongly dissipating turbulent mixing in the Sc model.

b. Discussion

The most significant uncertainty of all mixed layer models concerns details of the entrainment process and the shape of the "interface." This is particularly acute in Sc mixed-layer models because the cloud-top IR flux, which occurs in the vicinity of the interface, is an important turbulence-generating mechanism. In these models, the cloud-top is assumed to be flat, with a discontinuous inversion, and the positioning of the IR flux divergence controls the efficiency of the entrainment process (Stage and Businger, 1981b). In reality of course, the cloud top is not flat, nor is the inversion discontinuous (Deardorff *et al.*, 1980). The main results presented here, however, are relatively insensitive to these uncertainties.

An important topic relating to mixed-layer Sc modeling has been specifically avoided in this paper: this concerns the stability of the Sc deck (e.g., Deardorff, 1980). The calculations presented here concern the behavior of the surface and cloud-top heat budgets for Sc decks only. When the deck begins to break up, the fractional cloud cover becomes an important additional quantity, and because clear patches between clouds transmit substantially more sunlight to the ocean, it can be expected that the behavior of the ocean-surface heat budget will change radically with decreasing cloud coverage. The OST ranges used in Figs. 4–7 were chosen to maintain Sc stability. The cloud-top entrainment flux for the NH case with T_s = 291 K creates turbulence kinetic energy but the closure used here is not unstable in this case (see Stage and Businger, 1981b) in contrast to closures used by Deardorff (1976) and Randall (1980b). The criterion for cloud-top stability as discussed by Deardorff (1980) and Randall (1980a) is violated, so this case may not be realistic. On the other hand, Hanson (1982) has shown that this criterion may still be too restrictive and the issue is yet in doubt. It is to be hoped that future experimental work will address this cloud-top stability problem as well as provide an empirical basis for the heat budget calculations presented here.

Acknowledgments. Support from the Equatorial Pacific Ocean Climate Studies program of the National Oceanic and Atmospheric Administration is gratefully acknowledged, and HPH wishes to credit the congenial atmosphere at the Cooperative Institute for Marine and Atmospheric Studies, Miami, for stimulating this work. We would also like to thank E. J. Steiner for providing numerical regressions used in the calculations. Publication costs have been defrayed by NSF Grant ATM-80-2334.

REFERENCES

Cess, R. D., 1974: Radiative transfer due to atmospheric water vapor: Global consideration of the earth's energy balance. *J. Quant. Spectrosc. Radiat. Transfer,* **14,** 861–871.

——, 1976. Climate change: An appraisal of atmospheric feedback mechanisms employing zonal climatology. *J. Atmos. Sci.,* **33,** 1831–1843.

Deardorff, J. W., 1976. On the entrainment rate of a stratocumulus-topped mixed layer. *Quart. J. Roy. Meteor. Soc.,* **102,** 563–582.

——, 1980. Cloud top entrainment instability. *J. Atmos. Sci.,* **37,** 131–147.

——, and J. A. Businger, 1980. Comments on "Marine stratocumulus convection. Part I: Governing equations and horizontally homogeneous solutions." *J. Atmos. Sci.,* **37,** 481–482.

——, G. E. Willis and B. H. Stockton, 1980. Laboratory studies of the entrainment zone of a convectively mixed layer. *J. Fluid Mech.,* **100,** 41–64.

Fravalo, C., Y. Fouquart and R. Rosset, 1981: The sensitivity of a model of low stratiform clouds to radiation. *J. Atmos. Sci.,* **38,** 1049–1062.

Hanson, H. P., 1981: Note on stratocumulus instability. *Tellus.,* **33,** 109–112.

——, 1982. Note on mixed-layer entrainment closure. *J. Atmos. Sci.,* **39,** 470–473.

Hastenrath, S., and P. Lamb, 1978. *Heat Budget Atlas of the Tropical Atlantic and Eastern Pacific Oceans.* University of Wisconsin Press, 104 pp.

Ivanoff, A., 1977: Oceanic absorption of solar energy. *Modelling and Prediction of the Upper Layers of the Ocean,* E. B. Kraus, Ed., Pergamon, pp. 47–71.

Kahn, P. H., and J. A. Businger, 1979. The effect of radiative flux divergence on entrainment of a saturated convective boundary layer. *Quart. J. Roy Meteor. Soc.,* **105,** 303–306.

Kraus, H., and E. Schaller, 1978a. Steady-state characteristics of inversions capping a well-mixed planetary boundary layer. *Bound.-Layer Meteor.,* **14,** 83–104.

——, and ——, 1978b. A note on the closure in Lilly-type inversion models. *Tellus,* **30,** 284–288.

Lacis, A. A., and J. E. Hansen, 1974. A parameterization for the absorption of solar radiation in the earth's atmosphere. *J. Atmos. Sci.,* **31,** 118–133.

Lilly, D. K., 1968. Models of cloud-topped mixed layers under a strong inversion. *Quart. J. Roy. Meteor. Soc.,* **74,** 292–309.

——, and W. H. Schubert, 1980. The effects of radiative cooling in a cloud-topped mixed layer. *J. Atmos. Sci.,* **37,** 482–487.

Liou, K. N., and G. D. Wittman, 1979. Parameterization of the radiative properties of clouds. *J. Atmos. Sci.,* **36,** 1261–1273.

Niiler, P. P., and E. B. Kraus, 1977: One-dimensional models of the upper ocean. *Modelling and Prediction of the Upper Layers of the Ocean,* E. B. Kraus, Ed., Pergamon, pp. 143–172.

Oliver, D. A., W. S. Lewellen and G. G. Williamson, 1978. The interaction between turbulent and radiative transport in the development of fog and low-level stratus. *J. Atmos. Sci.,* **35,** 301–316.

Paltridge, G. W., 1980. Cloud radiation feedback to climate. *Quart. J. Roy. Meteor. Soc.,* **106,** 895–899.

Ramanathan, V., and J. A. Coakley, Jr., 1978. Climate modeling through radiative-convective models. *Rev. Geophys. Space Phys.,* **16,** 465–484.

Randall, D. A., 1980a. Conditional instability of the first kind upside-down. *J. Atmos. Sci.,* **37,** 125–130.

——, 1980b. Entrainment into a stratocumulus layer with distributed radiative cooling. *J. Atmos. Sci.,* **37,** 148–159.

Sasamori, T., 1968. The radiative cooling calculation for application to general circulation experiments. *J. Appl. Meteor.,* **7,** 721–729.

Schaller, E., and H. Kraus., 1978. Time-dependent inversions in different climatic regions. *Contrib. Atmos. Phys.,* **51,** 230–246.

——, and ——, 1981a. The role of radiation in an inversion-capped planetary boundary layer. Part I: The need for a detailed consideration of radiative processes. *Bound.-Layer Meteor.,* **20,** 485–495.

——, and ——, 1981b. The role of radiation in an inversion-capped planetary boundary layer. Part II: The internally interactive radiative-convective model. *Bound.-Layer Meteor.*, **20,** 497–513.

Schneider, S. H., 1972. Cloudiness as a global climatic feedback mechanism: The effects on the radiation balance and surface temperature of variations in cloudiness. *J. Atmos. Sci.*, **29,** 1413–1422.

——, and R. E. Dickinson, 1974. Climate modeling. *Rev. Geophys. Space Phys.*, **72,** 447–473.

——, and R. E. Dickinson, 1976. Parameterization of fractional cloud amounts in climatic models: The importance of modeling multiple reflections. *J. Appl. Meteor.*, **15,** 1050–1056.

——, W. M. Washington and R. M. Chervin, 1978. Cloudiness as a climatic feedback mechanism: Effects on cloud amounts of prescribed global and regional surface temperature changes in the NCAR GCM. *J. Atmos. Sci.*, **35,** 2207–2221.

Schubert, W. H., 1976. Experiments with Lilly's cloud-topped mixed layer model. *J. Atmos. Sci.*, **33,** 436–446.

——, J. S. Wakefield, E. J. Steiner and S. K. Cox, 1979a. Marine stratocumulus convection. Part I: governing equations and horizontally homogeneous solutions. *J. Atmos. Sci.*, **36,** 1286–1307.

——, ——, —— and ——, 1979b. Marine stratocumulus convection. Part II: Horizontally inhomogeneous solutions. *J. Atmos. Sci.*, **36,** 1308–1324.

Sellers, W. D., 1965. *Physical Climatology.* The University of Chicago Press, 272 pp.

Stage, S. A., and J. A. Businger, 1981a. A model for entrainment into a cloud-topped marine boundary layer: Part I: Model description and application to a cold air outbreak episode. *J. Atmos. Sci.*, **38,** 2213–2229.

——, and ——, 1981b. A model for entrainment into a cloud-topped marine boundary layer. Part II: Discussion of model behavior and comparison with other models. *J. Atmos. Sci.*, **38,** 2230–2242.

Steiner, E. J., and W. H. Schubert, 1976: Stratocumulus convection off the West Coast of South America. *Atmos. Sci. Pap. No. 270,* Colorado State University, Fort Collins, ISSN 0067-0340, 97 pp.

Stull, R. B., 1976: The energetics of entrainment across a density interface. *J. Atmos. Sci.*, **33,** 1260–1267.

Wakefield, J. S., and W. H. Schubert, 1981. Mixed layer model simulation of Eastern North Pacific stratocumulus. *Mon. Wea. Rev.*, **109,** 1952–1968.

Wetherald, R. T., and S. Manabe, 1980. Cloud cover and climate sensitivity. *J. Atmos. Sci.*, **37,** 1485–1510.

Winston, J. S., A. Gruber, T. I. Gray, Jr., M. S. Varnadore, C. L. Earnest and L. P. Mannello, 1979. Earth atmosphere radiation budget analysis derived from NOAA satellite. Date, June 1974–February 1978, Vol 1. Meteorological Satellite Laboratory, NOAA/NESS, U.S. Dept. Commerce, Washington, DC.